Version of Record: https://www.sciencedirect.com/science/article/pii/S0380133022000533
Manuscript_c82ad611251ea05dc63e03eee94c5ca7

A simple water clarity-turbidity index for the Great Lakes

Guangming Zheng[a,b,*], Paul M. DiGiacomo[a]

[a] *NOAA/NESDIS Center for Satellite Applications and Research, 5830 University Research Court, College Park, Maryland, 20740, U.S.A.*
[b] *Earth System Science Interdisciplinary Center, University of Maryland Research Park, 5825 University Research Court, College Park, Maryland, 20740, U.S.A.*

Abstract

There are a multitude of satellite-derived water clarity and turbidity indicators to support the decision making of environmental managers and policy makers. However, water quality dynamic ranges addressed by these indicators can differ significantly, subjecting non-expert users to potential pitfalls. Here we propose a satellite water clarity-turbidity index (CTI) as a simplified way to capture major changes in water clarity/turbidity across all water types in the Great Lakes. The CTI is defined to merge key information from three prerequisite variables derived from Visible Infrared Imaging Radiometer Suite (VIIRS) measurements, namely, the Secchi disk depth, the particulate backscattering coefficient, and the nephelometric turbidity, which are suitable for clear, intermediate, and turbid waters, respectively. Application to the Great Lakes shows that with one parameter, the CTI can illustrate major spatial and temporal patterns that are not entirely visible with each of the three original indicators alone. Using the CTI, we identified significant decrease in water turbidity in Lakes Michigan and Huron from 2000 to 2005, during which daily variability of CTI in August initially spiked and then gradually decreased most likely owing to diminishing whiting events. The CTI is a convenient and holistic assessment tool for water quality management.

Keywords: Satellite, remote sensing, water quality, Secchi disk depth, backscattering coefficient, nephelometric turbidity units

*Corresponding author
Email address: guangming.zheng@noaa.gov (Guangming Zheng)

1. Introduction

Water clarity and turbidity associated with light transmissivity are important water quality indicators that can be estimated from satellite data using various proxy variables. Commonly used proxies include the Secchi disk depth, Z_{sd}, the particulate backscattering coefficient, $b_{bp}(\lambda)$, diffuse attenuation coefficient of downwelling irradiance, $K_d(\lambda)$, and turbidity in nephelometric turbidity units (NTU), T_n (Zheng and DiGiacomo, 2017). It is important to note that no single variable fits all water types with respect to covarying with changes in water quality; each individual variable has an optimal dynamic range. For example, the Secchi Depth Z_{sd} is well suited for clear waters but its magnitude tends to diminish in turbid waters. With errors and uncertainties which are inherent to satellite data, highly turbid waters are practically indistinguishable using only Z_{sd}. For a similar reason, it is also difficult to evaluate turbidity of clear waters using the nephelometric turbidity T_n. Perhaps a good question to ask is, why estimate turbidity for waters with little turbidity, or likewise estimate clarity when there is essentially no clarity?

Therefore, effective application of these satellite products requires knowledge about their applicable dynamic range and what is actually "fit for purpose". This could overwhelm water quality managers and policy makers who may not have all the necessary technical expertise or more so the time to adequately research all available options. As a result, water quality managers often collect only those measurements proscribed by legal mandates, and typically these result predominantly if not solely from traditional field measurement programs. Although satellite data alone will not provide answers to all the issues or problems encountered by environmental managers and policy makers, space-based observations do provide invaluable synoptic coverage with frequent temporal revisits to robustly assess changes in environmental states (Schaeffer et al., 2013). Therefore, a simple but broadly applicable satellite-based product merging multiple variables might be more readily utilized and more informative for the decision making (Mouw et al., 2015). In practice, an effective, synergistic decision-making framework could include strategic leveraging of low-cost and timely satellite data to identify priority locations, followed by field sampling activities that target the priority locations to provide more precise and legally compliant measurements,

particularly at depth and also to provide parameters that cannot be measured from space (e.g., nutrients and pathogens). In other words, the satellite data provide routine and synoptic coverage, allowing for timely assessments of ecological changes, including identification of anomalous regional and local "hot-spots" and other areas that might warrant more in depth examination.

Towards this goal, we developed a framework that addresses the turbidity/clarity of a wide range of water types ranging from clear to highly turbid waters by merging Z_{sd}, $b_{bp}(\lambda)$, and T_n. The framework is demonstrated using data from the Great Lakes which is the largest surface freshwater system in the world by total area with great range of variability in water turbidity. In addition, the anthropogenic environment and aquatic ecosystems of the Great Lakes have in places and over time been impaired by pollution and invasive species; the CTI may facilitate and prioritize restoration activities.

2. Data and Methods

The remote-sensing reflectance, $R_{rs}(\lambda)$, data covering the Great Lakes region were obtained from three satellite missions: Visible Infrared Imaging Radiometer Suite (VIIRS)-SNPP (2011-2019), Moderate Resolution Imaging Spectroradiometer (MODIS)-Aqua (2002-2019), and MODIS-Terra (2000-2019). Daily Level-2 VIIRS-SNPP granule data with "science quality" were processed by the NOAA Ocean Color Science Team (reprocessing version, SCI_OC04.0_V1.21) and are available on the NOAA CoastWatch website (coastwatch.noaa.gov). Daily Level-2 MODIS-Aqua and -Terra data were obtained from the NASA's Goddard Space Flight Center Ocean Biology Processing Group using the Level 1&2 Browser on oceancolor.gsfc.nasa.gov. Data were reprocessed in 2018 (version "R2018.0"). Both VIIRS and MODIS data were produced with the atmospheric correction using a near-infrared band as the basis for making the "black-pixel" assumption. To avoid ice contamination, most data used in this study were collected during warm seasons from May to September unless otherwise noted.

As preprocessing, data were screened to remove quality issues and then gridded. Specifically, we rejected pixels flagged as high solar zenith (>75°) or high sensor zenith (>60°) angles, or high glint which is where sun glint radiance normalized by the solar irradiance that reaches sea level is greater than 0.01 Wang and Bailey (2001); Mikelsons and Wang (2019). In addition, the daily Level-2 data granules were reprojected into gridded format at 750-m (VIIRS) and 1000-m (MODIS) resolutions, respectively, and monthly

composites for each individual band were calculated as the mean of all gridded daily images in each month. The final product of this preprocessing is monthly 2-D arrays of the VIIRS $R_{rs}(\lambda)$ data at 410, 443, 486, 551, 638, and 671 nm, and MODIS $R_{rs}(\lambda)$ data at roughly identical bands, i.e., 412, 443, 469, 488, 547, 645, and 667 nm. Other MODIS ocean color bands were excluded from further calculations. Note that the VIIRS 638-nm band is not a regular ocean color band, but an "I-band" with 2 times higher spatial resolution and roughly 1/3 signal-to-noise ratio (SNR). So each $R_{rs}(638)$ value is aggregated from 4 I-band pixels and in this process its SNR is somewhat enhanced.

VIIRS [Chl-a] data are derived using an "OC3V" algorithm which is based on empirical reflectance ratio of blue-green bands available on VIIRS (Wang et al., 2017).

3. Results and Discussion

3.1. The Clarity-Turbidity Index

We propose a clarity-turbidity index (CTI) framework to provide a simple, qualitative measure of overall water quality across all Great Lakes waters ranging from clear to highly turbid. The CTI can be determined based on three satellite-derived variables, namely Z_{sd}, $b_{bp}(550)$, and T_n. In theory, these variables quantify different optical properties of water. When measured in the field or laboratory Z_{sd} is affected by both light absorption and scattering, whereas $b_{bp}(550)$ and T_n are only or mostly determined by light scattering in the backward and side angles. In the context of remote sensing, however, the magnitude of R_{rs} and everything derived from it are affected by both absorption and scattering, including the three variables discussed here. What is more important is to select a set of variables that can serve as robust indicators of total suspended matter for a broad range of water quality. In this regard, the three variables, Z_{sd}, $b_{bp}(550)$, and T_n, are carefully selected to account for clear, intermediate, and turbid waters, respectively, which also correspond to the general water types when uncertainties of these variables are the lowest. Below, we explain each variable in details and describe how the CTI framework is designed to ensure that the adopted information always comes from the variable with the lowest uncertainty.

There are many formulas to derive these three variables from $R_{rs}(\lambda)$ (e.g., for Z_{sd}, see Doron et al., 2011; Lee et al., 2015; Son and Wang, 2020, and references cited therein). Users of our approach may select the most appropriate

formulas as they see fit. For the purpose of demonstrating the framework of CTI, here we use a widely adopted formula given by Lee et al. (2015) to derive Z_{sd}:

$$Z_{sd} = \frac{1}{2.5K_d(\lambda_{min})} \ln\left(\frac{\mid 0.14 - R_{rs}(\lambda_{min}) \mid}{0.013}\right) \quad (1)$$

, where $K_d(\lambda)$ is the vertically averaged spectral diffuse attenuation coefficient, and λ_{min} is the light wavelength with minimum $K_d(\lambda)$, i.e., where light can penetrate the deepest into the water column. Following Lee et al. (2015), $K_d(\lambda)$ was calculated from the spectral light absorption, $a(\lambda)$, and backscattering coefficients, $b_b(\lambda)$, which were calculated with the Quasi-Analytical Algorithm (QAA) version 6 (Lee et al., 2013).

Although the accuracy of this Z_{sd} algorithm may require further validation in turbid waters (e.g., Yin et al., 2021), for clear waters with Z_{sd} >10 m which is its main application scenario here, the percent-wise agreement among various other Z_{sd} algorithms were shown to be better (Doron et al., 2011), i.e., less uncertainties in general to use satellite-derived Z_{sd} compared with turbid waters. For clear waters, this algorithm were demonstrated to work well for waters from a broad geographical range (the US and China) (Lee et al., 2015).

The particulate $b_{bp}(550)$ is calculated simply by subtracting the pure water contribution, $b_{bw}(550)$, from the QAA-derived total $b_b(550)$. The QAA has been demonstrated to perform consistently well for a wide range of waters with intermediate turbidity across the world (Zheng et al., 2014; Mitchell et al., 2014; Pitarch et al., 2020), and therefore tuning of QAA for the Great Lakes intermediate waters is not essential. In fact, a refinement effort of QAA using field data collected from Lake Superior yielded only negligible improvement (Mouw et al., 2013). Note that the 550 nm here is a nominal band name referring to the 551 nm for VIIRS and 547 nm for MODIS. The pure water contribution $b_{bw}(550)$ is calculated with the Water Optical Properties Processor (WOPP) developed by Rottgers et al. (2011). In this calculation water salinity was set to zero, and water temperature to 10 °C which is close to the medians of monthly whole-lake average temperature of individual Great Lakes from May to September (see coastwatch.glerl.noaa.gov/statistic/).

To calculate turbidity in nephelometric units, T_n, we used a formula based on the magnitude of $R_{rs}(645)$ (or 638 nm for VIIRS) from Dogliotti et al. (2015):

$$T_n = \frac{228.1\pi R_{rs}(645)}{1 - \pi R_{rs}(645)/0.1641} \quad (2)$$

This formula was based on data from a diverse set of environments (European and South American coastal waters). In addition, it converges with other regression relationships obtained for various turbid water bodies in the world between T_n and $R_{rs}(645)$ (see Fig. 9 in Zheng and DiGiacomo, 2017). This suggests that eq. 2 is robust and can be applied to the Great Lakes with relatively low uncertainty.

We also examined the use of T_n derived from reflectance at near-infrared (IR) bands (e.g., 860 nm) to account for more turbid waters but found it unnecessary because such waters are rare in the Great Lakes except outside of episodic sediment plume and algal bloom events. However, in many other coastal and inland waters where turbidity are much higher to the extent that R_{rs} at the 645-nm band is also saturated and no longer responding to turbidity variations, it is necessary to use a near-IR band to derive T_n more accurately (e.g., Dogliotti et al., 2015). This would require an atmospheric correction scheme using a shortwave-infrared band as a basis for making the "black-pixel" assumption.

Given Z_{sd}, $b_{bp}(550)$, and T_n, the CTI is determined based on threshold values of these variables as illustrated in Table 1 and Fig. 1A. Figure 1A shows the distribution of all monthly VIIRS data used in this study which comprise over two million samples. The MODIS data show similar patterns except that the T_n rarely exceeds 60 NTU (not shown). The first step is to separate the two endmember groups, i.e., clear waters and turbid waters. This is important because turbidity indicator T_n diminishes in clear waters and clarity indicator Z_{sd} diminishes in turbid waters, and as they diminish, they also lose the dynamic range to capture the variability of water quality (see right end of blue points and left end of red points in Fig. 1A). Based on the VIIRS data distribution, two threshold values of $b_{bp}(550)$, 0.01 and 0.1 m^{-1}, were selected to broadly categorize a given pixel into clear (CTI $\leq$4), intermediate (CTI 5), or turbid waters (CTI $\geq$6). The value of 0.01 m^{-1} happens to intercept with the upper bound of $Z_{sd} - b_{bp}(550)$ distribution at $Z_{sd} \approx$10 m, whereas the value of 0.1 m^{-1} happens to intercept with the upper bound of $T_n - b_{bp}(550)$ distribution at $T_n \approx$15 NTU. Therefore Z_{sd}=10 m is used as a threshold value to further separate the clearest (CTI$\leq$3) from the transitional clear-intermediate waters (CTI=4), and T_n =15 NTU is used to separate the intermediate-turbid (CTI=6) from the most turbid waters (CTI$\geq$7). For the clearest waters (CTI 1 through 3), the CTI is based solely on Z_{sd} with threshold values of 15 and 20 m, respectively; whereas for the most turbid waters (CTI 8 through 11), it is based solely on T_n with threshold

values of 30, 60, 100, 200, and 500 NTU, respectively. There are relatively few data points beyond 200 NTU so they were not shown in Fig. 1A to better illustrate other CTI indices.

The selection of these threshold values may make the CTI approach appear arbitrary; nevertheless, it is the framework merging critical information from Z_{sd}, $b_{bp}(550)$, and T_n that is important. The CTI approach is essentially a discretization of Z_{sd}, $b_{bp}(550)$, and T_n data in their most applicable turbidity ranges. It transforms quantitative into qualitative information, while distilling and preserving dominant water quality information out of an overwhelmingly large amount of data, making it suitable for water quality managers and policy-makers to readily grasp general trends and patterns in both space and time. In addition, the way CTI is defined makes it a flexible approach. First, its applicable range of clarity/turbidity can be easily expanded; it could potentially cover much clearer (Gieskes et al., 1987; Doron et al., 2011; Lee et al., 2018, e.g., oceanic waters with Z_{sd} as deep as 70 m,) and much more turbid waters (Dogliotti et al., 2015, e.g., T_n over 1000,). However, caution must be taken when dealing with special cases such as waters with high turbidity or high concentrations of dissolved organic matter because the relationships among satellite-derived Z_{sd}, $b_{bp}(550)$, and T_n may depart significantly from those shown in Fig. 1A. Second, the choices of threshold values are flexible; users can easily change these thresholds as they see fit and easily trace each CTI back to the ranges of Z_{sd}, $b_{bp}(550)$, and T_n through Table 1. The adjustment of various threshold values for Great Lakes waters can be made without the need to analyze additional satellite data. A user can simply make changes based on their own knowledge, e.g., beyond what T_n value poses a concern for environmental compliance, or in a trial-and-error fashion by keep tuning thresholds and examining the resultant CTI maps until the most insightful CTI patterns show up. In essence, the CTI provides a one-number metric for water quality managers and policy-makers to make quick evaluations without having to worry about technical details, particularly for regions where turbidity variation is large.

With respect to covering a large range of water turbidity/clarity, the combination of Z_{sd}, $b_{bp}(550)$, and T_n is a rather unique choice because replacing either Z_{sd} or $b_{bp}(550)$ with other variables commonly used for clear to moderately turbid waters does not yield equally satisfying result. For example, we tried to use the mean surface diffuse attenuation coefficient, $K_d(490)$, in lieu of Z_{sd} or $b_{bp}(550)$ but the distribution of data points is much less converged (Fig. 1B and C). Note that the $K_d(490)$ data used here are provided in the

Index	Water type	$Z_{sd}[m]$	$b_{bp}(550)[m^{-1}]$	Turbidity [NTU]
1	Clear-3	20−25		
2	Clear-2	15−20		
3	Clear-1	10−15		
4	Clear-Intermediate	0−10	<0.01	
5	Intermediate		0.01−0.1	
6	Intermediate-Turbid		>0.1	<15
7	Turbid-1			15−30
8	Turbid-2			30−60
9	Turbid-3			60−100
10	Turbid-4			100−200
11	Turbid-5			200−500
12	Turbid-6			>500

Table 1: Definitions of clarity-turbidity indices based on satellite-derived Z_{sd}, $b_{bp}(550)$, and T_n. Blank means the corresponding variable is not used to define a specific index.

standard Level-2 VIIRS products from NOAA, which was derived following the approach by Wang et al. (2009) as opposed to the formula used to derive Z_{sd} (Lee et al., 2015) shown above. In addition, water quality as indicated by $K_d(490)$ is often inconsistent with that by Z_{sd}, $b_{bp}(550)$, and T_n, e.g., data points with high $K_d(490)$ (suggesting high turbidity) but low $b_{bp}(550)$ (suggesting low turbidity) (Fig. 1B), or low $K_d(490)$ (suggesting low turbidity) but low Z_{sd} (suggesting high turbidity) (Fig. 1C). Such inconsistency on top of the large data spread makes it difficult to use $K_d(490)$ to define CTI in a robust fashion (Fig. 1A).

Using the approach discussed above we mapped out the CTI for the Great Lakes using $R_{rs}(\lambda)$ data from VIIRS-SNPP, MODIS-Aqua and -Terra, and made monthly composites for each sensor. Compared with Z_{sd}, $b_{bp}(\lambda)$, and T_n individually, the CTI exhibits a broader range of variability. Taking VIIRS data in Arpil 2018 for example (Fig. 2), among the three original variables the clearest waters in central Lake Huron (white dashed circles) can only be seen in the Z_{sd} map, the most turbid waters in Lake Erie (black dashed circles) can only be seen in the T_n map, whereas the $b_{bp}(550)$ map only highlights turbidity changes in moderately turbid waters (e.g., the Saginaw Bay, gray dashed cicles). In contrast, the CTI map shows all main features across all

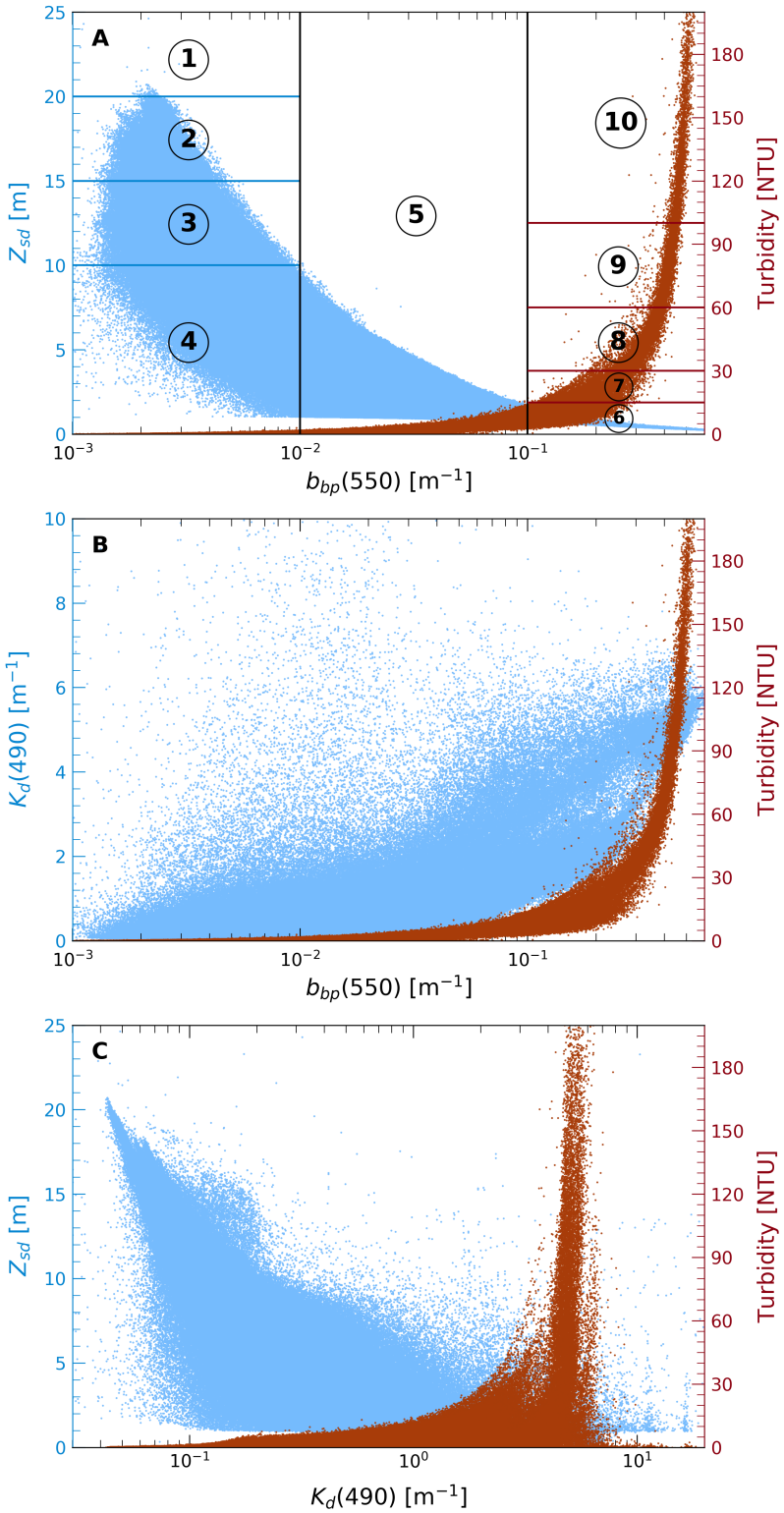

Figure 1: (A) VIIRS-SNPP monthly averaged Z_{sd}, $b_{bp}(550)$, and T_n data in the Great Lakes during 2012-2019 overlaid with clarity-turbidity indices (denoted by circled numbers). See Table 1 for numerical definitions. For comparison, an alternative variable, $K_d(490)$, is used to replace Z_{sd} (B) or $b_{bp}(550)$ (C).

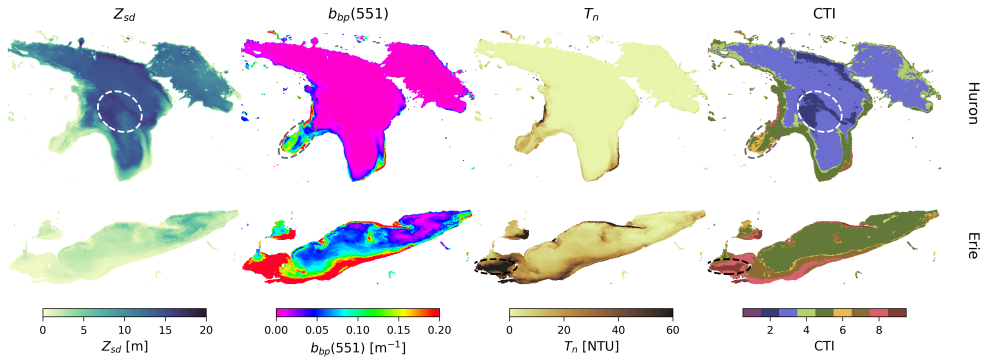

Figure 2: Comparison between maps of VIIRS-derived Z_{sd}, $b_{bp}(\lambda)$, and T_n and the CTI using Lakes Huron and Erie in April 2018 as an example.

water types ranging from the clearest to the most turbid.

3.2. General Trends

Next, we examined the consistency of CTI derived from VIIRS-SNPP, MODIS-Aqua and -Terra by comparing the CTI values derived from the 3 different sensors. For brevity we selected one month from each season (spring, summer, and fall) and calculated the lakewide average CTI. Figure 3 shows that the agreement among the three sensors is generally very good particularly for the two MODIS sensors which exhibit almost identical results. VIIRS-derived CTI values are systematically larger than the MODIS counterparts but they generally follow the same trend, except a few outliers such as Lake Superior in September 2014 and Lake Ontario in September 2015 which are associated with significantly different spectral shapes in VIIRS- and MODIS-derived $R_{rs}(\lambda)$. The difference between VIIRS and MODIS data are associated with the different atmospheric correction schemes used, as indicated by a sensitivity test we did (not shown). In addition, the difference may also arise from the saturation of MODIS over bright water targets (e.g. Land et al., 2018). Nonetheless, the inter-sensor disagreement represents only a small fraction of the entire dataset. Overall, the results suggest that for clear and intermediate waters the CTI can be considered independent from sensor, algorithm, and data-processing system. For turbid waters the VIIRS- and MODIS-derived CTIs can be significantly different owing to the smaller dynamic range exhibited in the MODIS 645-nm band.

Figure 3 also shows that from the whole-lake standpoint, water quality in Lakes Michigan and Huron exhibits significant decadal changes. In particular, dramatic CTI drop occurred around 2004, consistent with previous studies (e.g. Binding et al., 2015). Average CTI in May dropped from >4 in 2002−2003 to ∼3.5 in 2005 for Lakes Michigan and Huron (Fig. 3D,G). Average CTI in Lake Michigan dropped even more significantly in September than in May from >4.5 in 2001 to ∼3.5 in 2005 (Fig. 3F), but the same trend did not happen in Lake Huron. Another significant trend is found in July, when CTI kept dropping since 2000, reached the minimum in 2012 with a total drop of ∼0.8, and bounced back by a total of ∼0.7 as of 2019 (Fig. 3E,H). A similar trend was also found in Lake Superior in May (Fig. 3A), although the magnitude of variation is much smaller. Otherwise, CTI changes in the other three lakes, i.e., Lakes Superior, Erie, and Ontario over the past two decades (2000-2019) are mostly associated with interannual variability. Interestingly, Lake Ontario exhibits both the largest (in September, Fig. 3O) and the smallest (in July, Fig. 3N) interannual variability.

To further examine spatial patterns of water quality changes, we obtained quinquennial CTI maps using mean Z_{sd}, $b_{bp}(550)$, and T_n calculated every five years (Fig. 4). For this analysis we used only MODIS-Terra data which provides the longest time record (2000−2019). Note that MODIS-derived T_n tends to be underestimated at higher turbidity levels compared with VIIRS. However, this is a minor issue for the purpose of this study because very turbid waters only account for a negligible portion of the Great Lakes. Figure 4 confirms that the most significant change in CTI occurred in Lake Michigan and Huron and between the two periods of 2000−2004 and 2005−2009. Most areas in Lakes Michigan and Huron underwent a CTI drop by 1, and the biggest drop occurred in September in central southern Lake Michigan with a CTI drop by 2, from 5 (intermediate) to 3 (clear-1) (Fig. 4C,F). After this significant drop in water turbidity, Lake Huron and southern Lake Michigan continued to clear up during 2010−2019 whereas CTI of northern Lake Michigan stabilized. An intriguing spatial pattern is the decrease in CTI at relatively shallow locations in May. For example, the location of the clear waters with CTI = 2 in Lakes Michigan and Huron (dark blue in Fig. 4G,J) matches roughly with shallow bathymetry contours (not shown). This pattern might be associated with higher fraction of the water column cleared per day by invasive dreissenid mussels (Rowe et al., 2015), and in particular by quagga mussels in Lake Michigan (Nalepa et al., 2020) and Huron (Nalepa et al., 2018). The relationship between CTI and invasive mussels needs to be

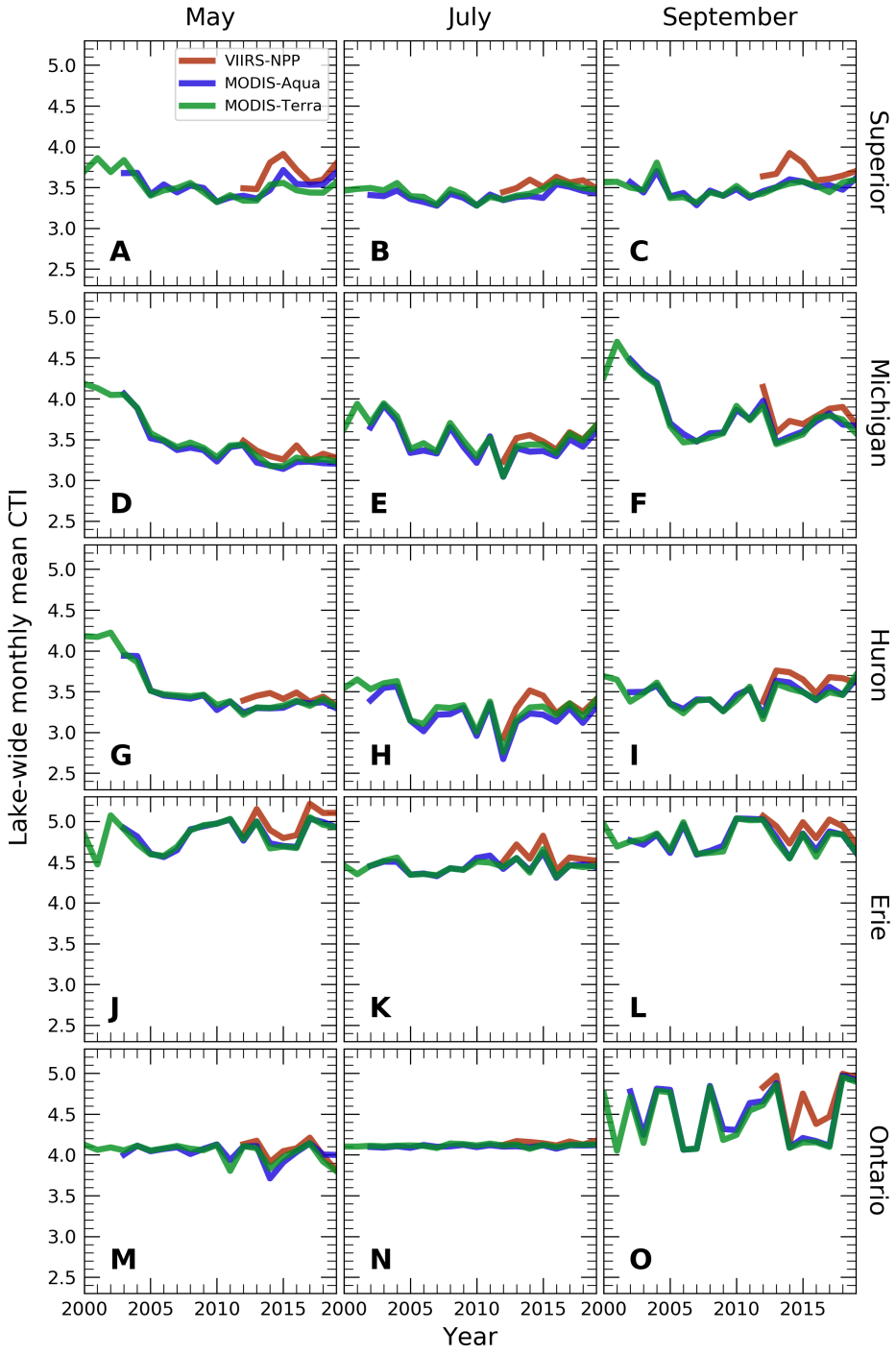

Figure 3: Lake-by-lake monthly mean clarity-turbidity index from 2000 to 2019 for May, July, and September.

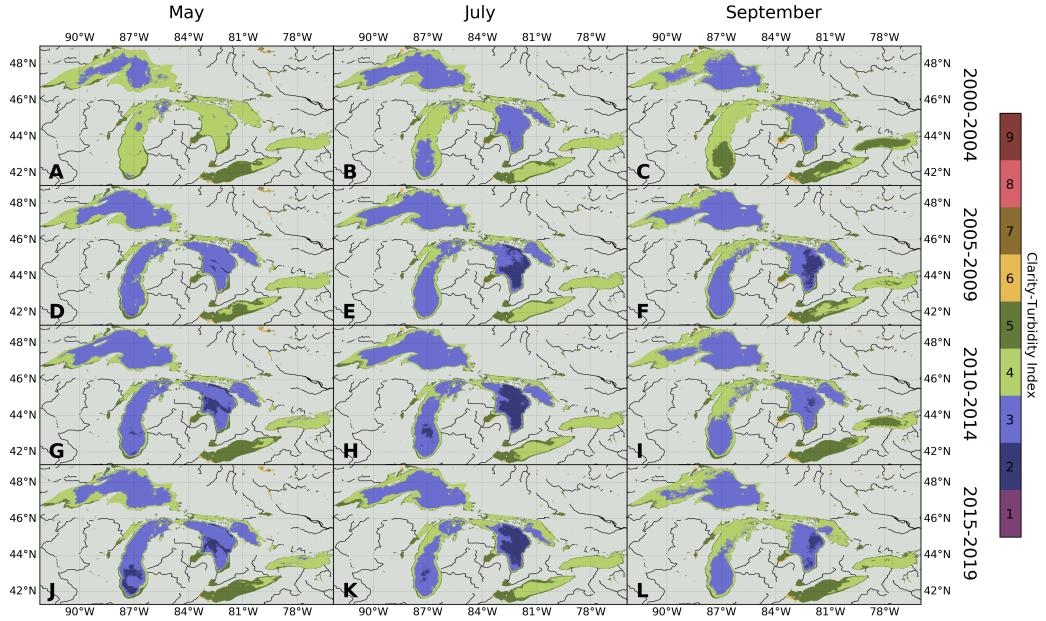

Figure 4: Quinquennial climatology of water clarity-turbidity index of the Great Lakes across spring, summer, and fall.

further investigated in future studies.

3.3. Case Studies

In the previous section we used monthly composite data to highlight long-term trends of water quality changes in the Great Lakes. Water quality managers are also interested to understand short-term water quality variability of waterbodies under their jurisdiction, which can be very dynamic. In this section, we conduct two case studies to demonstrate the use of CTI to studying water quality variability on a day-to-day basis. To characterize this variability we tested several statistical metrics calculated for all daily data sampled at each pixel within each month, which include the standard deviation, the 1st-99th interpercentile range, and the 1st-3rd interquartile range. After comparing features shown in these three error parameters, the interquartile range, hereafter referred to as $Q_3 - Q_1$, was selected as the metric to measure temporal variability of CTI, which gives a robust measurement of the spread of daily retrievals without being subjected to the influence of potential noise.

After examining the monthly time series of CTI $Q_3 - Q_1$ from 2000 to

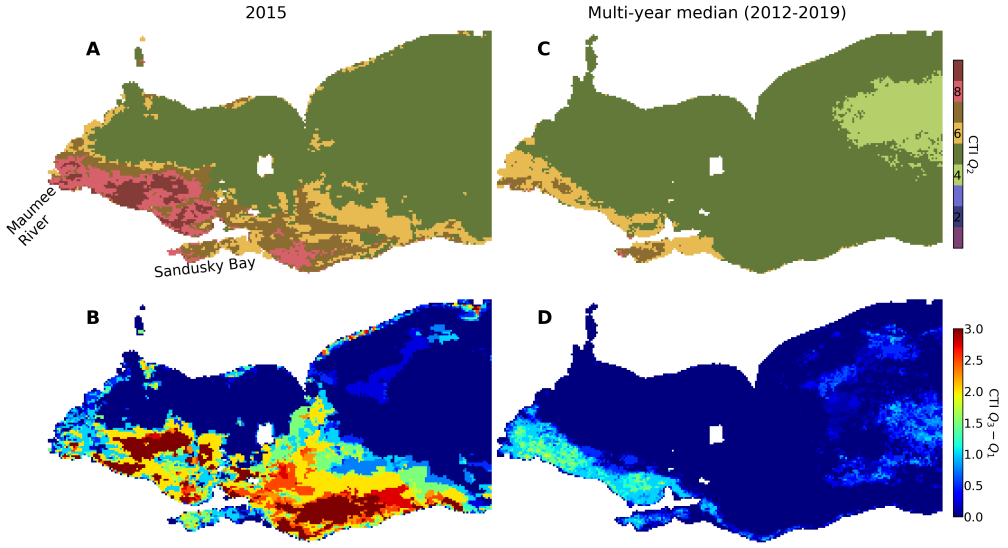

Figure 5: June median (A) and interquartile range (B) of daily CTI in western Lake Erie in 2015 derived from VIIRS-SNPP, compared with normal conditions as represented by the multi-year medians values of the same variables (C and D). See Fig. 6 for symbol definitions.

2019, we noticed two regions with large CTI fluctuations: Western Lake Erie and Southern Lake Michigan. In June 2015, Western Lake Erie exhibited abnormally high CTI in terms of both magnitude and variability (Fig. 5A,B) compared with normal levels (Fig. 5C,D). Median CTI reached 9 off the Maumee River mouth, whereas in normal years it is only 5. Daily variability of CTI represented by $Q_3 - Q_1$ exceeded 3 off the Maumee River mouths and off the Sandusky Bay, compared to near zero in normal years. The dramatic change in 2015 can be explained by significantly increased river discharge in this area. For example, monthly mean streamflow of the Maumee River was record-high in June 2015 (the 3rd greatest since 1939) (Stumpf et al., 2016), which delivered significant amount of suspended sediments to Lake Erie.

In Southern Lake Michigan, August CTI exhibited a regime shift from 2000 to 2005, shifting from steadily Clear-Intermediate (4) to steadily Clear-1 type (3) (top and middle panels in Fig. 6). During this period, both the magnitude (top panel) and the variability ($Q_3 - Q_1$, middle panel) of CTI had an initial surge in 2001 and then gradually decreased in the following years. These trends cannot be explained by annual changes in [Chl-a] level (bot-

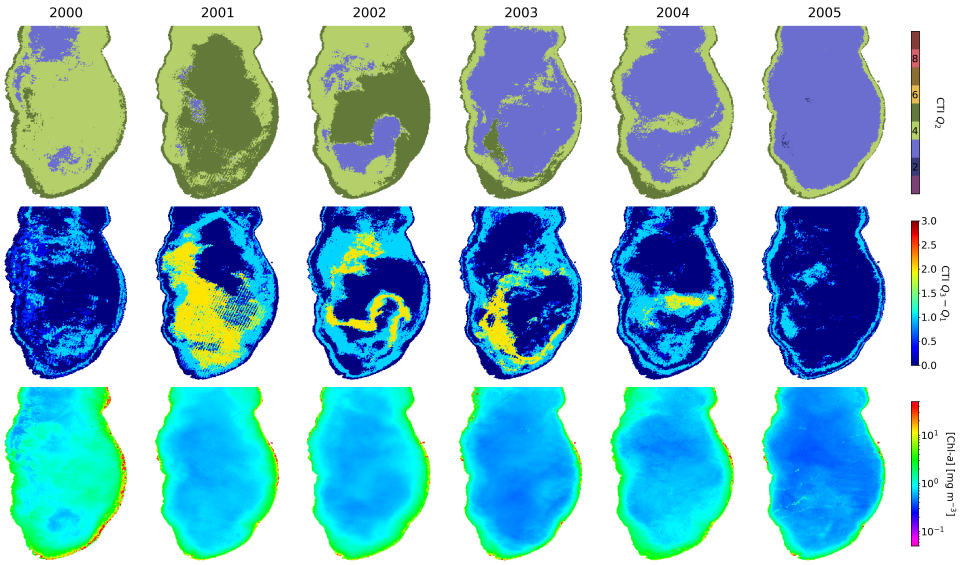

Figure 6: Monthly median (top panel) and interquartile range (middle panel) of daily clarity-turbidity index CTI derived from MODIS-Terra, in comparison to [Chl-a] (bottom panel) in southern Lake Michigan in August from 2000 to 2005. Q_1, Q_2, and Q_3 are the first, second, and third quartiles of all daily retrievals of the month.

tom panel) which sometimes changed in the opposite way relative to CTI. For instance, between 2000 and 2001 mean [Chl-a] in August decreased while median CTI increased. However, this trend must be interpreted with caution because the [Chl-a] here is derived from a reflectance band ratio algorithm and is subject to contamination by other pigmented matter such as colored dissolved organic matter. The most likely contributor to the trends in CTI is most likely attributable to changes in frequency of whiting events, waters laden with clouds of small calcite particles formed by precipitation of calcium carbonate. In fact, true color images of Lake Michigan whiting events in 1999 and 2001 were highlighted by NASA Earth Observatory as "Image of the Day" on September 18, 2001 (earthobservatory.nasa.gov/images/1768). Historically, whiting events were common in Lake Michigan during warm seasons in the 1970s (Strong and Eadie, 1978). However, X-ray scanning analyses made for suspended particulate samples collected in Lake Michigan in summer 2008, 2010, and 2012 show no indication of whiting events (Effler et al., 2013; Peng and Effler, 2015); specifically, either total suspended particulate concentration or contribution of calcium carbonate to the total are very low compared with typical whiting event levels. To the best of our knowledge, whiting events in Southern Lake Michigan have not been reported since 2001. Our results suggest that whiting events in Southern Lake Michigan underwent a gradual decline during 2001−2005 (Fig. 6). The

2001 whiting events could well be the very last major episode of the whiting "show" in Lake Michigan.

It is worth noting that the regime shift of CTI is accompanied by a reduction of [Chl-*a*] (lower panel, Fig. 6), although the two variables are not strongly correlated. The timing of these changes matches well with the rapid expansion of quagga mussels in Lake Michigan from 2000 to 2005 (Nalepa et al., 2020). It is highly likely that the filtering effect of quagga mussels leads to both the regime shift of CTI and the reduction of phytoplanton biomass. Dreissenid mussels can reduce the frequency and/or intensity of whiting events through direct calcium uptake (Barbiero et al., 2006). They could also alter whiting events by changing the abundance of cyanobacteria which are recognized as key players in the precipitation of calcium carbonate in marine and freshwater systems (Thompson and Des Marais, 1997; Dittrich and Sibler, 2010; Kamennaya et al., 2012). Cyanobacteria promote whiting events by creating alkaline microenvironment surrounding the cells, serving as nucleation sites (Thompson and Des Marais, 1997), and exuding polysaccharides that have a strong potential to exchange protons with the surrounding environment (Dittrich and Sibler, 2010). More research is needed to answer the question of what mechanisms caused the decline of whiting events in Lake Michigan.

4. Summary

The CTI developed here is a simple approach to make an approximate evaluation of water turbidity or clarity for any type of optically deep water body, i.e., as long as the water-leaving light is unaffected by reflection off the water bottom. It allows the evaluation of water quality to be "approximately right", as opposed to "precisely wrong" which may result from the adoption of a variable that is inappropriate for the waters of interest. Application of this approach to satellite data essentially generates dynamic water quality thematic maps from which significant water quality changes can be detected. However, CTI alone does not tell what is causing those changes; it should be viewed as an "alarm bell" warning that something is happening and is worth more in-depth examination with the aid of other sources of information. In this study, we show that the use of CTI allows the depiction of spatial gradients and temporal trends of water quality in the Great Lakes, and major turbidity drops in Lake Michigan and Lake Huron around 2004, a timing that matches the start of lake-wise infestation of invasive dreissenid mussels. We

also show that significant day-to-day variation in water turbidity can arise from high river streamflow and diminishing whiting events.

The CTI could be extended to other water bodies in the world, particularly for regions where water clarity/turbidity spans a great range. Note that the CTI definition and the relationships among Z_{sd}, $b_{bp}(550)$, and T_n shown here (Fig. 1A, Table 1) only serve as an example. To achieve the most effective result, especially for waters with extreme optical properties such as high dissolved organic absorption, high suspended mineral concentration, high algal biomass, etc, it is recommended to redefine CTIs with new thresholds using remote-sensing data from the region of interest and based on practical needs of local water quality managers. In addition, caution must also be taken to ensure the quality of input data of $R_{rs}(\lambda)$ for those optically complex waters. We recommend the CTI approach to water quality managers and policy-makers whose intention is to seek holistic understanding from satellite data rather than conducting detailed quantitative analyses with them.

Acknowledgment

This work was supported by the Great Lakes Restoration Initiative (GLRI). Datasets for this research are freely available from coastwatch.noaa.gov and oceancolor.gsfc.nasa.gov, for which we are grateful. The contents of this article are solely the opinions of the authors and do not constitute a statement of policy, decision, or position on behalf of the NOAA or the U.S. Government.

References

Barbiero, R.P., Tuchman, M.L., Scott Millard, E., 2006. Post-dreissenid increases in transparency during summer stratification in the offshore waters of lake ontario: Is a reduction in whiting events the cause? Journal of Great Lakes Research 32, 131 – 141. doi:10.3394/0380-1330(2006)32[131:PIITDS]2.0.CO;2.

Binding, C.E., Greenberg, T.A., Watson, S.B., Rastin, S., Gould, J., 2015. Long term water clarity changes in north america's great lakes from multi-sensor satellite observations. Limnology and Oceanography 60, 1976–1995. doi:10.1002/lno.10146.

Dittrich, M., Sibler, S., 2010. Calcium carbonate precipitation by cyanobacterial polysaccharides. Geological Society, London, Special Publications 336, 51–63. doi:10.1144/SP336.4.

Dogliotti, A., Ruddick, K., Nechad, B., Doxaran, D., Knaeps, E., 2015. A single algorithm to retrieve turbidity from remotely-sensed data in all coastal and estuarine waters. Remote Sensing of Environment 156, 157 – 168. doi:10.1016/j.rse.2014.09.020.

Doron, M., Babin, M., Hembise, O., Mangin, A., Garnesson", P., 2011. Ocean transparency from space: Validation of algorithms estimating secchi depth using meris, modis and seawifs data. Remote Sensing of Environment 115, 2986 – 3001. doi:10.1016/j.rse.2011.05.019.

Effler, S.W., Peng, F., O'Donnell, D.M., Strait, C., 2013. The backscattering coefficient and its components in the great lakes: A review and synthesis. Journal of Great Lakes Research 39, 108 – 122. URL: http://www.sciencedirect.com/science/article/pii/S0380133013000099, doi:10.1016/j.jglr.2013.02.002.

Gieskes, W.W.C., Veth, C., Woehrmann, A., Graefe, M., 1987. Secchi disc visibility world record shattered. Eos, Transactions American Geophysical Union 68, 123–123. doi:10.1029/EO068i009p00123-01.

Kamennaya, N.A., Ajo-Franklin, C.M., Northen, T., Jansson, C., 2012. Cyanobacteria as biocatalysts for carbonate mineralization. Minerals 2, 338–364.

Land, P.E., Shutler, J.D., Smyth, T.J., 2018. Correction of sensor saturation effects in modis oceanic particulate inorganic carbon. IEEE Transactions on Geoscience and Remote Sensing 56, 1466–1474. doi:10.1109/TGRS.2017.2763456.

Lee, Z., Arnone, R., Boyce, D., Franz, B., Greb, S., Hu, C., Lewis, M., Schaeffer, B., Shang, S., Wang, M., et al., 2018. Global water clarity: continuing a century-long monitoring. Eos 99. doi:10.1029/2018EO097251.

Lee, Z., Hu, C., Shang, S., Du, K., Lewis, M., Arnone, R., Brewin, R., 2013. Penetration of uv-visible solar radiation in the global oceans: Insights from ocean color remote sensing. Journal of Geophysical Research: Oceans 118, 4241–4255. doi:10.1002/jgrc.20308.

Lee, Z., Shang, S., Hu, C., Du, K., Weidemann, A., Hou, W., Lin, J., Lin, G., 2015. Secchi disk depth: A new theory and mechanistic model for underwater visibility. Remote Sensing of Environment 169, 139 – 149. doi:10.1016/j.rse.2015.08.002.

Mikelsons, K., Wang, M., 2019. Optimal satellite orbit configuration for global ocean color product coverage. Opt. Express 27, A445–A457. doi:10.1364/OE.27.00A445.

Mitchell, C., Cunningham, A., McKee, D., 2014. Remote sensing of shelf sea optical properties: Evaluation of a quasi-analytical approach for the irish sea. Remote Sensing of Environment 143, 142–153. doi:10.1016/j.rse.2013.12.011.

Mouw, C.B., Chen, H., McKinley, G.A., Effler, S., O'Donnell, D., Perkins, M.G., Strait, C., 2013. Evaluation and optimization of bio-optical inversion algorithms for remote sensing of lake superior's optical properties. Journal of Geophysical Research: Oceans 118, 1696–1714. doi:10.1002/jgrc.20139.

Mouw, C.B., Greb, S., Aurin, D., DiGiacomo, P.M., Lee, Z., Twardowski, M., Binding, C., Hu, C., Ma, R., Moore, T., Moses, W., Craig, S.E., 2015. Aquatic color radiometry remote sensing of coastal and inland waters: Challenges and recommendations for future satellite missions. Remote Sensing of Environment 160, 15 – 30. doi:10.1016/j.rse.2015.02.001.

Nalepa, T.F., Burlakova, L.E., Elgin, A.K., Karatayev, A.Y., Lang, G.A., Mehler, K., 2020. Abundance and biomass of benthic macroinvertebrates in lake michigan in 2015, with a summary of temporal trends. doi:10.25923/g0d3-3v41. technical Memorandum.

Nalepa, T.F., Riseng, C.M., Elgin, A.K., Lang, G.A., 2018. Abundance and distribution of benthic macroinvertebrates in the lake huron system: Saginaw bay, 2006-2009, and lake huron, including georgian bay and north channel, 2007 and 2012. doi:10.25923/aqe2-ma69. technical Memorandum.

Peng, F., Effler, S.W., 2015. Light-absorbing properties of mineral particles in the great lakes. Journal of Great Lakes Research 41, 573 – 583. doi:10.1016/j.jglr.2015.03.028.

Pitarch, J., Bellacicco, M., Organelli, E., Volpe, G., Colella, S., Vellucci, V., Marullo, S., 2020. Retrieval of particulate backscattering using field and

satellite radiometry: Assessment of the qaa algorithm. Remote Sensing 12. doi:10.3390/rs12010077.

Rottgers, R., Doerffer, R., McKee, D., Schonfeld, W., 2011. Algorithm Theoretical Basis Document: The Water Optical Properties Processor (WOPP). Technical Report. Tech. rep., Helmholtz-Zentrum Geesthacht, University of Strathclyde, Geesthacht.

Rowe, M.D., Obenour, D.R., Nalepa, T.F., Vanderploeg, H.A., Yousef, F., Kerfoot, W.C., 2015. Mapping the spatial distribution of the biomass and filter-feeding effect of invasive dreissenid mussels on the winter-spring phytoplankton bloom in lake michigan. Freshwater Biology 60, 2270–2285. doi:10.1111/fwb.12653.

Schaeffer, B.A., Schaeffer, K.G., Keith, D., Lunetta, R.S., Conmy, R., Gould, R.W., 2013. Barriers to adopting satellite remote sensing for water quality management. International Journal of Remote Sensing 34, 7534–7544. doi:10.1080/01431161.2013.823524.

Son, S., Wang, M., 2020. Water quality properties derived from viirs measurements in the great lakes. Remote Sensing 12. doi:10.3390/rs12101605.

Strong, A.E., Eadie, B.J., 1978. Satellite observations of calcium carbonate precipitations in the great lakes1. Limnology and Oceanography 23, 877–887. doi:10.4319/lo.1978.23.5.0877.

Stumpf, R.P., Johnson, L.T., Wynne, T.T., Baker, D.B., 2016. Forecasting annual cyanobacterial bloom biomass to inform management decisions in lake erie. Journal of Great Lakes Research 42, 1174 – 1183. doi:10.1016/j.jglr.2016.08.006.

Thompson, Joel B., S.L.S.B.T.J., Des Marais, D.J., 1997. Whiting events: Biogenic origin due to the photosynthetic activity of cyanobacterial picoplankton. Limnology and Oceanography 42, 133–141. doi:10.4319/lo.1997.42.1.0133.

Wang, M., Bailey, S.W., 2001. Correction of sun glint contamination on the seawifs ocean and atmosphere products. Appl. Opt. 40, 4790–4798. doi:10.1364/AO.40.004790.

Wang, M., Liu, X., Jiang, L., Son, S., 2017. Visible Infrared Imaging Radiometer Suite (VIIRS) Ocean Color Products. Technical Report. College Park, MD.

Wang, M., Son, S., Harding Jr., L.W., 2009. Retrieval of diffuse attenuation coefficient in the chesapeake bay and turbid ocean regions for satellite ocean color applications. Journal of Geophysical Research: Oceans 114. doi:10.1029/2009JC005286.

Yin, Z., Li, J., Liu, Y., Xie, Y., Zhang, F., Wang, S., Sun, X., Zhang, B., 2021. Water clarity changes in lake taihu over 36 years based on landsat tm and oli observations. International Journal of Applied Earth Observation and Geoinformation 102, 102457. doi:10.1016/j.jag.2021.102457.

Zheng, G., DiGiacomo, P.M., 2017. Uncertainties and applications of satellite-derived coastal water quality products. Prog Oceanogr 159, 45 – 72. doi:10.1016/j.pocean.2017.08.007.

Zheng, G., Stramski, D., Reynolds, R.A., 2014. Evaluation of the quasi-analytical algorithm for estimating the inherent optical properties of seawater from ocean color: Comparison of arctic and lower-latitude waters. Remote Sensing of Environment 155, 194–209. doi:10.1016/j.rse.2014.08.020.

Highlights

A simple water clarity-turbidity index for the Great Lakes

Guangming Zheng, Paul M. DiGiacomo

- A framework to extract water quality information from satellite data is proposed.
- The approach is applicable to a wide range of water types ranging from clear to turbid.
- It is a convenient tool to identify main changes in water quality with one single parameter.